analytical chemistry

pubs.acs.org/ac Article

Direct Infusion-Three-Dimensional-Mass Spectrometry Enables Rapid Chemome Comparison among Herbal Medicines

Xia Xu, Wei Li, Ting Li, Ke Zhang, Qingqing Song, Li Liu, Pengfei Tu, Yitao Wang, Yuelin Song,* and Jun Li*

Cite This: *Anal. Chem.* 2020, 92, 7646−7656 Read Online

ACCESS | Metrics & More | Article Recommendations | Supporting Information

ABSTRACT: Direct infusion-mass spectrometry (DI-MS) currently serves as an alternative analytical tool for metabolomics owing to the unique high-throughput advantage. Except the inherent shortcoming at a significant matrix effect, there are two other primary technical obstacles dampening its wide applications, such as data alignment and structural annotation. To address these two obstacles, a novel strategy termed as DI-three-dimensional-MS (DI-3D-MS) was proposed here, and chemome comparison among several confusing herbal medicines (HMs) belonging to the *Umbelliferae* family was conducted as a proof-of-concept. Each test sample was directly infused into Qtrap-MS. In the first dimension, stepwise multiple ion monitoring (MIM) program was implemented to universally acquire the quantitative information on all HMs and to generate aligned data files. In the second dimension, MS^2 spectra were universally recorded by enhanced product ion (EPI) experiments that were triggered by MIM via an information-dependent acquisition algorithm. In the third dimension, online energy-resolved MS (ER-MS) was programmed to yield breakdown graphs for all MIM items. Moreover, a data library was built to aid structural identification by involving MS^2 and CE_{50} features that were obtained by well-developed LC−MS methods. Qualitative and quantitative potentials of DI-3D-MS were validated toward metabolomics study. Significant species differences were observed, and all materials were grouped into three clusters. After matching MS^2 spectra and breakdown graphs between DI-3D-MS and those in the data library, coumarins ubiquitously existed in each HM, and angular-type pyranocoumarins, linear-type pyranocoumarins, angular-type furanocoumarins, along with ligustilide derivatives offered primary contributions for the classification pattern. Above all, DI-3D-MS is an eligible choice for rapid metabolomics of HMs and other matrices as well.

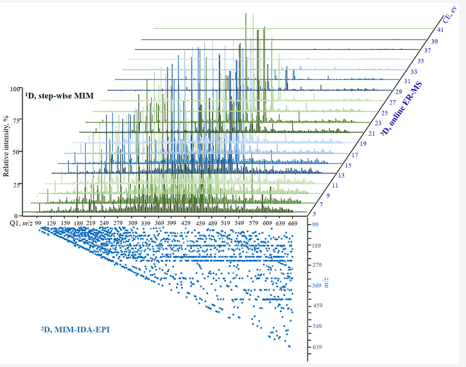

Although less popular than LC−MS, direct infusion-MS (DI-MS, also known as flow injection-MS and direct injection-MS) occupies the front rank of analytical tools that are suitable for metabolomics studies,[1−4] because MS, in particular high-resolution MS, is able to record, theoretically, the quantitative information on all charged ions. Owing to being free of time-consuming chromatographic separations, DI-MS owns a unique high-throughput advantage. However, direct infusion is exactly like a two-edged sword because a significant matrix effect intrinsically accompanies the efficient measurements. Moreover, there are two other primary technical barriers, such as signal alignment and structural annotation, when applying DI-MS toward a rapid metabolomics study. Because it is almost impossible to completely address this native matrix effect shortcoming, attempts are therefore made here to circumvent the other two obstacles via proposing a versatile strategy.

In the case of LC−MS-based metabolomics, e.g., LC−Qtof-MS, the variables are usually output as t_R−m/z pairs and retention time (t_R) acts as the calibrator for data alignment.[5−8] However, DI-MS cannot provide t_R for any ion feature, and mass shifts[9,10] frequently occur within different analytical runs, leading to a challenging workload to omit redundant information as well as the substrate signals. To break through this bottleneck calls for an approach enabling the generation of each data file with constant size, and the signal alignment procedure is then totally eliminated. Being inspired by the fact that the analytical program of targeted metabolomics always yields each data file containing an identical amount of variables, a pseudotargeted metabolomics concept has been raised by Prof. Xu's group through developing a robust selected reaction monitoring (SRM) approach on LC−QqQ-MS that is capable of monitoring all metabolites found by the survey measurements on LC−Qtof-MS.[11−14] Moreover, multiple ion monitoring (MIM) mode that is carried out by defining Q1 = Q3 ion transitions has been claimed to demonstrate

Received: February 3, 2020
Accepted: May 5, 2020
Published: May 5, 2020

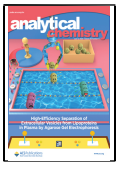

https://dx.doi.org/10.1021/acs.analchem.0c00483
Anal. Chem. 2020, 92, 7646−7656

comparable sensitivity with SRM,[15−17] and a stepwise MIM program allows for the quantitative information acquisition of almost all metabolites in given matrices.[18] Consequently, a stepwise MIM strategy might offer an opportunity for globally quantitative information recording and then outputing all data files containing an equal number of variables when samples are directly injected into a MS.

High-quality multistage mass spectra are the prerequisites of confirmatively structural annotation, and the powerful databases (e.g., MyCompoundID,[19,20] HMDB,[21] MassBank,[22] etc.) then facilitate linking m/z values to identities. In comparison of data-independent MS^2 acquisition technologies, such as SWATH[23] and MS(E),[24] the information-dependent acquisition (IDA, also known as data-dependent acquisition), e.g., enhanced product ion (EPI) scan on hybrid triple quadrupole-linear ion trap-MS (Qtrap-MS), is advantageous at unambiguously affiliating fragment ion species to their precursors,[25,26] which is extremely important when a mass of ions arrives at the MS at the meantime. Because each compound is continuously injected into MS for DI-MS measurement, rather than a narrow peak (just like a single pulse) corresponding to LC−MS, enough time is available, fortunately, to acquire MS^2 spectra for all ions-of-interest according to triggering a large panel of EPI events.

Inquiring multistage mass spectral signals to those well-developed databases cannot achieve unambiguously structural annotation because isomers are widely present in the plant kingdom. Auxiliary evidence is therefore mandatory. Fortunately, the collision energy (CE) at which the survival yield is 50% (CE_{50}) that is able to differentiate isomers is the exact orthogonal molecular descriptor for MS^2 signals,[27,28] notably when stepwise MIM is programmed for quantitative information acquisition. Many ion transitions as demanded are permitted by DI-MS to enter a monitoring list, and CE_{50} values of all MIM ion transitions (actually the Q1 ions) can be gained even in a single measurement by applying online energy-resolved MS (ER-MS).[27,29] Afterward, structural annotation confidence will be significantly boosted, if a database containing MS^2 spectral and CE_{50} properties for each identity is available.

In order to rapid acquire qualitative and quantitative information, a so-called DI-three-dimensional-MS (DI-3D-MS) strategy is proposed by involving the aforementioned techniques, such as MIM (1st dimension), MIM-IDA-EPI (2nd dimension), and online ER-MS (3rd dimension), which are responsible for gaining quantitative information, MS^2 spectra, and CE_{50}, respectively. There are a number of herbal medicines (HMs) derived from *Umbelliferae* plants. This HM cluster frequently owns similar appearances and fragrances and ubiquitously contains coumarins. Isomers have been extensively disclosed in *Umbelliferae* plants.[30−32] Although belonging to an identical family, each HM exhibits unique therapeutic features attributing to the different chemome patterns, such as qualitative and quantitative properties. Therefore, an in-depth chemome comparison among a set of confusing HMs, such as Angelicae sinensis Radix (the dried roots of *Angelica sinensis*), Angelicae dahuricae Radix (the dried roots of *Angelica dahurica*), Angelicae decursiva Radix (the dried roots of *Angelica decursiva*), Peucedani Radix (the dried roots of *Peucedanum praeruptorum*), and Peucedani pubescens Radix (the dried roots of *Peucedanum pubescens*) was conducted to illustrate and evaluate the applicability of DI-3D-MS toward rapid chemome comparison. The findings in the current study are envisioned to point out the chemical markers for each species and, more importantly, to demonstrate DI-3D-MS to be a promising choice for a high-throughput metabolomics study, beyond HMs.

EXPERIMENTAL SECTION

Chemicals and Materials. LC−MS grade ACN, methanol, and formic acid were purchased from Thermo-Fisher (Pittsburgh, PA). The deionized water (18.2 MΩ) was prepared in-house by a Milli-Q Integral water purification device (Millipore, MA).

Thirty batches of dried herbal roots, in total, were collected from Beijing Tongrentang Co. Ltd. (Beijing, China) and Anguo medicinal materials market (Anguo, China). All raw materials were carefully authenticated by one of the authors (Prof. P.F. Tu), an experienced pharmacognosist, on the basis of the well-defined macroscopic along with microscopic features documented in the Chinese Pharmacopeia (2015 Edition).[33] The original sources included *Angelica sinensis* (AS1−AS6), *Angelica dahurica* (AD1−AD4), *Angelica decursiva* (also known as *Peucedanum decursivum*, PD1−PD8), *Peucedanum praeruptorum* (PR1−PR11), and *Peucedanum pubescens* (PP1). All voucher specimens (Nos. SYL-2019-1 ∼ SYL-2019-30) were deposited in our institute. Icariin was commercially obtained from Standard Biotech Co. Ltd. and acted as the internal standard (IS).

Sample Preparation. All raw materials (AS1−AS6, AD1−AD4, PD1−PD8, PR1−PR11, and PP1) were individually grinded into powders and sieved through an appropriate mesh. Approximately 1.0 g of the powders was sampled from each batch and accurately weighed. Ultrasonic-assisted extraction was conducted for the powders using 50 volumes (g/mL) of 70% aqueous methanol for 30 min. Each extract underwent 10 000g centrifugation and filtration through a 0.22 μm Nylon membrane, successively. IS solution (3 μg/mL) was prepared by dissolving icariin with 70% aqueous methanol. Two groups (I and II) of test samples were prepared for different objectives.

Group I samples participated in DI-stepwise MIM measurements to generate quantitative data set for metabolomics. A 1 mL aliquot was sampled from each filtrate and individually fortified with 150 μL of IS solution to yield 30 samples (AS1−AS6, AD1−AD4, PD1−PD8, PR1−PR11, and PP1). Moreover, an equal volume (300 μL) of each filtrate was pooled, and an 8 mL portion of the resultant mixture was thoroughly mixed with 1.2 mL of IS solution to yield the quality control (QC) sample.

Group II samples were implemented for both MIM-IDA-EPI and online ER-MS assays to yield qualitative information. A 0.5 mL aliquot was sampled from each filtrate and pooled within each species to generate homogenized samples, five in total, for all species. The QC sample was also involved in MIM-IDA-EPI and online ER-MS measurements.

DI-3D-MS Measurement. A 5500Qtrap mass spectrometer (SCIEX, Foster City, CA) equipped with a Turbo V ESI source was deployed to monitor the eluent from PEEK tubing linking to a syringe pump (KDS 100, KD Scientific, Holliston, MA). Because most compounds in HMs-of-choice favored positive ionization polarity,[31,32,34,35] merely the positive mode was ticked for the ion source. The following ion source settings were applied: GS1, 10 psi; GS2, 10 psi; CUR, 20 psi; ion-spray needle voltage, + 5500 V; heater gas temperature, 150 °C; and collisionally-activated dissociation gas, high level. Unit

https://dx.doi.org/10.1021/acs.analchem.0c00483
Anal. Chem. 2020, 92, 7646−7656

resolution (0.6−0.8 Da) was applied for either a Q1 or Q3 chamber. The flow rate of 10 μL/min was maintained for each assay, and at injection intervals, the PEEK tubing was completely washed by delivering the vehicle solvent (75% aqueous methanol) at a flow rate of 100 μL/min for 2 min. At the beginning of each assay, the vehicle in the tubing entered the MS to generate the background region.

DI-Stepwise MIM Measurement. All Group I samples were measured by DI-stepwise MIM program. Notably, the QC sample was analyzed after every three samples. Owing to the lack of nitrogen compounds (mainly alkaloids) in the selected HMs, most quasi-molecular ions, mainly protonated molecular ions ($[M + H]^+$), should be odd numbers. The step-size was thereby defined as 2 Da,[36] and fortunately, the redundant information resulted from the isotopic ions would be omitted. The range was defined as m/z 99−669. Subsequently, a set of MIM ion transitions, such as m/z 99 = 99, 101 = 101, and so on for 285 ones in total, were typed into the monitoring list. The collision energy (CE) as 5 eV was defined for each ion transition, and declustering potential was always set as 100 V. IS was monitored by m/z 677 > 515 with CE as 30 eV. Worthily, the dwell time as 100 ms was assigned to each ion transition to suppress instrumental noise, and each cycle would last 0.5 min. Four minutes, corresponding to eight cycles, was set for each measurement.

DI-MIM-IDA-EPI Assay. Each Group II sample was measured by DI-MIM-IDA-EPI. In order to record MS^2 spectrum for each MIM ion transition, an entire assay was divided into a panel of periods. MIM-IDA-EPI mode[37] was applied for each segment containing eight ion transitions along with eight EPI experiments. The criterion termed as *top*-8 most abundant ion transitions was applied for each IDA algorithm, and all Q1 ions would be trapped, actually, in the linear ion trap (LIT) chamber to generate MS^2 spectra. The CE and its spread (CES) were maintained as 35 and 30 eV, respectively, for each EPI scan. The scan range as m/z 50−700 and scan rate as 20 000 Da/s was applied for each EPI experiment.

DI-Online ER-MS Experiment. All homogenized samples participated in DI-online ER-MS measurements to comprehensively gain breakdown graphs. Each MIM ion transition derived a set of pseudoion transitions (PITs).[27] Each PITs set containing 19 PITs exactly corresponded to a panel of progressive CEs among 5−41 eV containing 19 CE levels (e.g., 5, 7, 9, and so on). For instance, PITs such as m/z 99.001 = 99.001, 99.002 = 99.002, 99.003 = 99.003, and so on for 19 ones in total were produced by m/z 99 = 99, and they were assigned with 5, 7, 9 eV, and so on, accordingly. Therefore, a total of 5415 items were obtained and dispersed into three periods of a single acquisition program, because at most 2500 items were allowed in a single monitoring list. Each dwell time was also defined as 100 ms to ensure the data quality.

In-House Data Library Construction. Each Group II sample was also measured by the routine LC−MS program to build an in-house data library. Chromatographic separations were conducted on a CAPCELL CORE C_{18} column (2.1 mm × 150 mm, 2.7 μm, Shiseido, Tokyo, Japan). The mobile phase consisting of 0.1% aqueous formic acid (A) and ACN (B) was delivered at a total flow rate of 0.3 mL/min in a gradient as follows: 0−12 min, 15%−60% B; 12−18 min, 60−70% B; 18−20 min, 70%−90% B; 20−20.1 min, 90%−15% B; and 20.1−25 min, 15% B. The column oven was maintained at 40 °C, and injection volume was set as 2.0 μL.

Shimadzu IT-TOF MS equipped with an ESI interface was in charge of recording high-resolution multistage mass spectra by applying the defaulted parameter settings.[30] Qtrap-MS was subsequently deployed to obtain CE_{50} values for all detected compounds, 178 in total (Table S1);[27] after that, the LC−IT-TOF-MS data set was well processed. Regarding CE_{50} acquisition, briefly, the quasi-molecular ions (e.g., $[M + H]^+$ or $[M + Na]^+$) of all detected compounds were involved to generate $Q_1 = Q_3$ ion transitions (Table S1) and each ion transition subsequently created a set of PITs that were assigned with progressive CEs (step-size as 2 eV and range as 5−41 eV). Taking praeruptorin A (128 in Table S1) for instance, the quasi-molecular ion was detected at m/z 409 ($[M + Na]^+$), and ion transition of m/z 409 = 409 afterward generates a set of CE-tagged PITs, such as m/z 409.001 = 409.001 at 5 eV, m/z 409.002 = 409.002 at 7 eV, m/z 409.003 = 409.003 at 9 eV, and so on.

Data Analysis. SCIEX Analyst software (Version 1.6.2) was responsible for outputting all signal intensities. For each sample in Group I, the intensities of all ion transitions, including the one for IS, were imported into Microsoft Office Excel after deducting the substrate region (Phase I in Figure S1). The intensity of each MIM was then normalized by IS response to yield a data column. The columns of all samples, including QC sample columns, were combined to generate a ".csv" file for metabolomics. Principal component analysis (PCA) was afterward conducted using SIMCA-P software (Version 14.0, Umetrics, Umeå, Sweden); following that, all variables were Pareto-scaled.

For each sample in Group II, the intensities of each PITs set were normalized by the greatest one to generate a data file. All data files were then imported into GraphPad Prism 7.0 software (San Diego, CA) to construct the regressive breakdown graphs. The CE_{50} value of each MIM ion transition corresponded to 50% relative intensity.

RESULTS AND DISCUSSION

Chemical Characterization and Data Library Construction. All homogenized samples were subjected onto LC−IT-TOF-MS to characterize their chemical profiles. All chromatograms are illustrated in Figure S2. Each data file was then analyzed carefully to translate the signals in each chromatogram into chemical structures via applying the mass fragmentation pathways as well as the tandem mass spectral information archived in the literature.[30−32,38] After in-depth data processing, a total of 178 components, mainly coumarins, were structurally identified. Owing to the lack of authentic compounds, all identities were tentatively characterized. The chromatographic and tandem mass spectral information as well as the putative identities are summarized in Table S1. The distribution pattern of each annotated signal is also illustrated in Table S1. Ligustilide derivatives served as the primary chemical family for Angelicae sinensis Radix,[38] and Angelicae dahuricae Radix was rich of linear-type furanocoumarins.[32] Angelicae decursiva Radix contained linear-type furanocoumarins, linear-type pyranocoumarins, and angular-type furanocoumarins.[31] Angular-type pyranocoumarins were enriched by either Peucedani Radix[30] or Peucedani pubescens Radix.

Peucedani Radix for instance, 63 components in total, were tentatively characterized and most of them were derived from a khellactone scaffold by bearing acyl group(s) at C-3′ and/or C-4′ position(s) (Figure S3A). When the protonated molecular ion ($[M + H]^+$) was transmitted for collision induced

https://dx.doi.org/10.1021/acs.analchem.0c00483
Anal. Chem. 2020, 92, 7646−7656

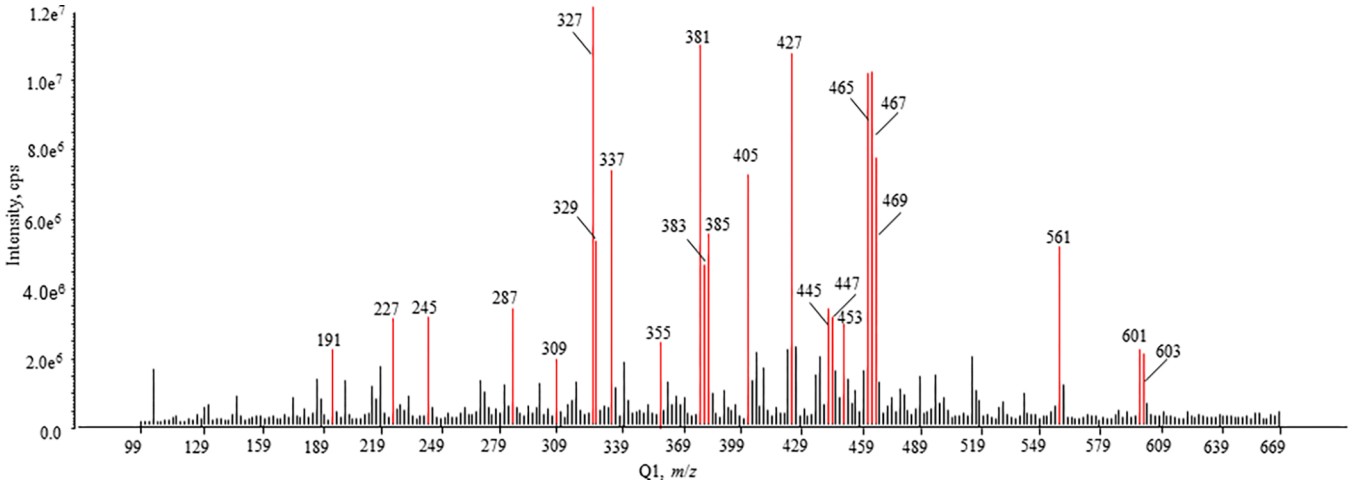

Figure 1. Stepwise MIM fingerprint of the quality control sample.

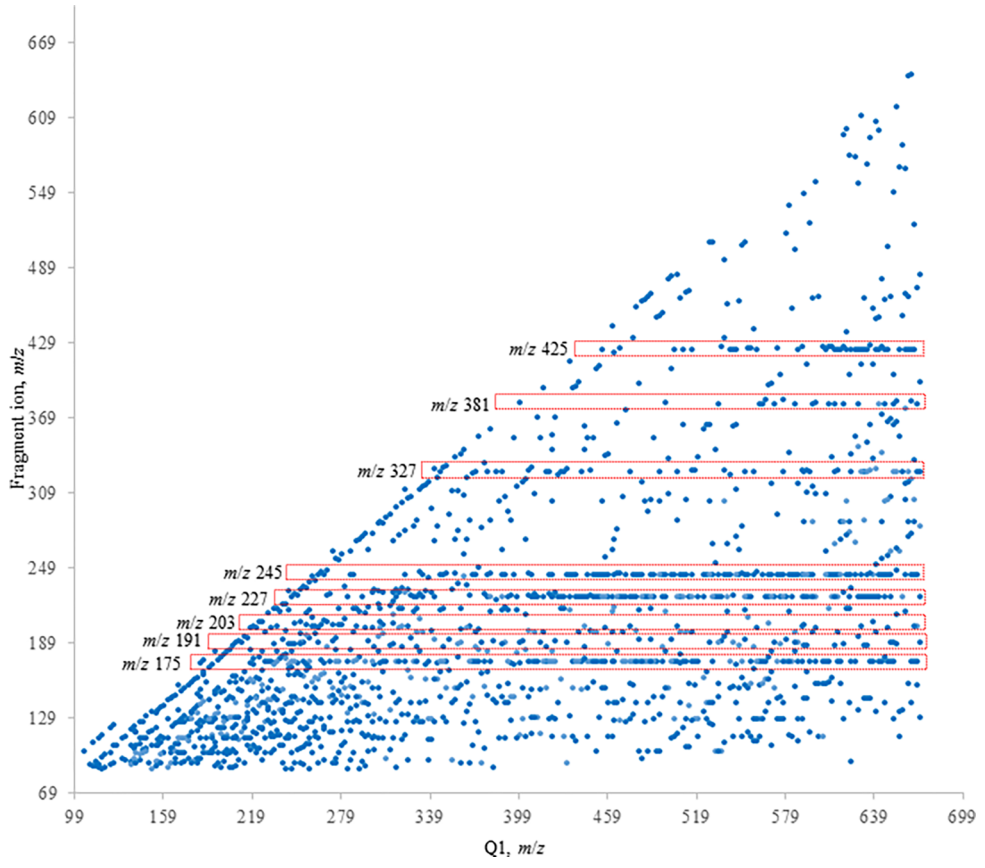

Figure 2. Primary ion features generated from all enhanced product ion experiments triggered by stepwise MIM survey experiments through an information-dependent acquisition manner. Signals with great occurrence rates, such as *m*/*z* 175, 191, 203, 227, 245, 327, 381, and 425, are highlighted.

dissociation, neutral cleavages of RCOOH, R′COOH, (R−H)CO, and/or (R′−H)CO occurred to generate the so-called diagnostic fragment ions at *m*/*z* 245 and 227 (Figure S3A).[34] Moreover, further dissociation might occur for these ions to yield signal at *m*/*z* 203 according to C_3H_6 neutral loss from C-2′ position.[34]

Afterward, the quasi-molecular ions, mainly $[M + H]^+$ ions, of all 178 compounds were subjected to CE_{50} acquisition on Qtrap-MS. After importing the normalized response data file of each PIT set into Graphpad Prism software, all CE_{50} values calculated from those regressive sigmoid curves are summarized in Table S1. Most values varied among 10−30 eV. It was worthy to note that isomers usually gave out similar fragment ion profiles and, nonetheless, different CE_{50} features. Taking praeruptorin A (128) vs. pteryxin (129), a pair of *regio*-isomers, for instance, both yielded fragment ion species such as *m*/*z* 327, 245, and 227, whereas significant differences occurred for their CE_{50} values (praeruptorin A, 21.27 eV vs. pteryxin, 21.86 eV). Therefore, CE_{50} might be a complementary structural descriptor for fragment ion species and vice versa. The in-

https://dx.doi.org/10.1021/acs.analchem.0c00483
Anal. Chem. 2020, 92, 7646−7656

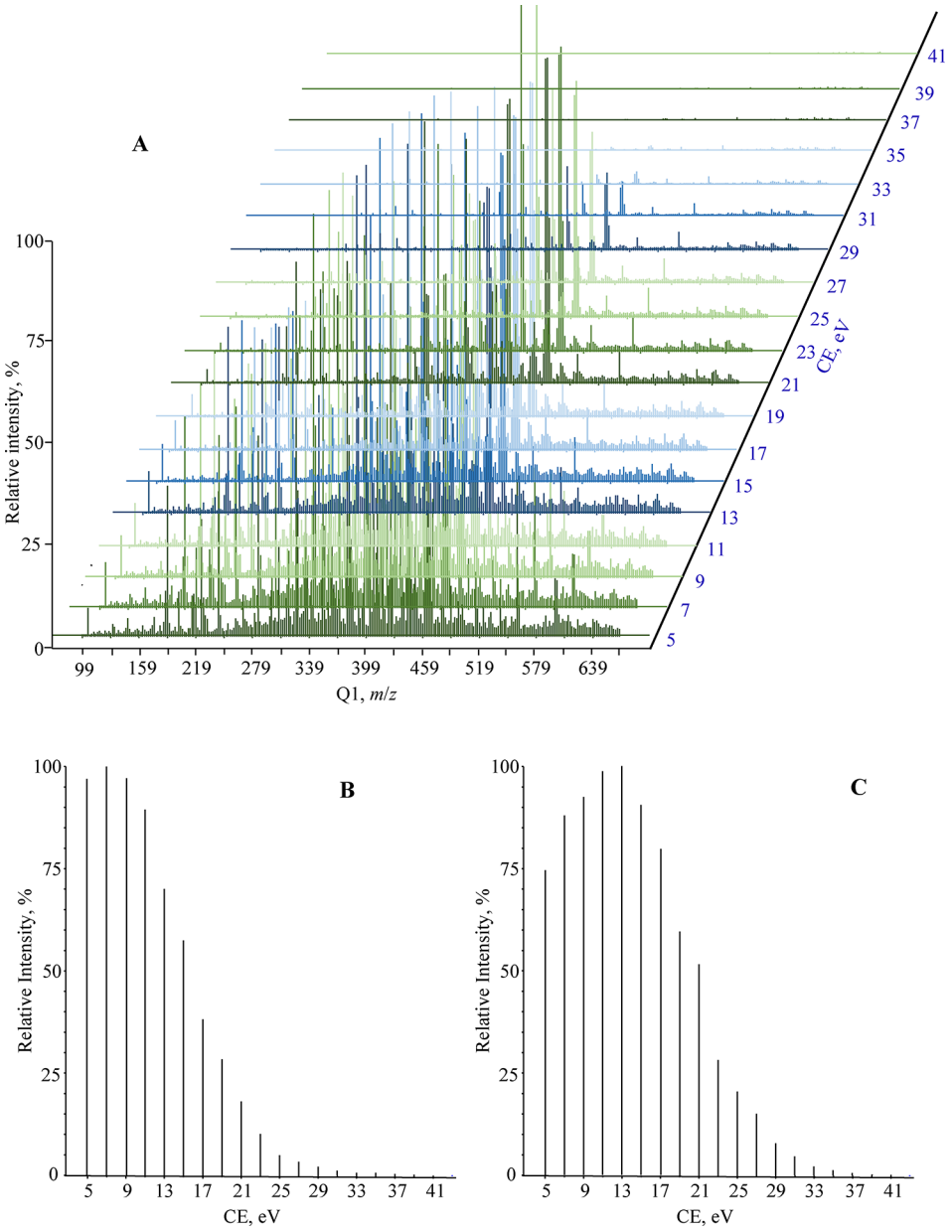

Figure 3. (A) Overlaid stepwise MIM fingerprints of quality control sample vs. progressive collision energy (step size, 2 eV; range, 5−41 eV). (B and C) Relative response vs. progressive collision energy (step size, 2 eV; range, 5−41 eV) of *m*/*z* 381 (B) and *m*/*z* 227 (C).

house data library (Table S1) was thereafter built by involving MS^2 spectrum and breakdown graph of each plausible identity.

Assessment of Quantitative and Qualitative Performances. The QC sample was implemented to evaluate the quantitative and qualitative performances of DI-3D-MS strategy. The quantitative data set was yielded by DI-stepwise MIM. Regarding an entire assay, the total ion current chromatogram could be fragmented into three phases, Phases I−III (Figure S1). The vehicle in the tubing first entered the MS to generate the substrate range (Phase I), the subsequent climbing phase corresponded to the mixed vehicle and the QC sample (Phase II), and the stable phase (Phase III) finally took place after that the tubing was completely equilibrated. The chromatograms of six QC measurements are overlaid as Figure S1. Obviously, satisfactory performance in terms of precision occurred. Moreover, the quantitative data set that was generated by deducting the average intensity profile of Phase I from that of Phase III was also implemented to evaluate the intensity variation of each MIM ion transition. As expected, RSDs (%) of all ion transitions were lower than 7.3%. The representative MIM fingerprint of QC sample is exhibited in Figure 1. The primary signals were observed at *m*/*z* 191, 227, 245, 287, 309, 327, 329, 337, 355, 381, 383, 385, 405, 409, 413, 417, 427, 445, 447, 453, 465, 467, 469, 561, 601, and 603 (only show Q1 ions). After inquiring these signals in Table S1, *m*/*z* 191, 381, 383, and 385 were tentatively assigned to ligustilide derivatives and *m*/*z* 227, 245, 287, 309, 327, 329, 405, 409, 427, 445, 447, 465, and 467 were plausibly originated from angular-type pyranocoumarins, linear-type pyranocoumarins, and angular-type furanocoumarins, whereas the other signals could not be annotated.

The flow rate of the syringe pump that governed the analyte amount entering the ion source was carefully optimized by balancing the sensitivity and upper limits of quantitation. A low

https://dx.doi.org/10.1021/acs.analchem.0c00483
Anal. Chem. 2020, 92, 7646−7656

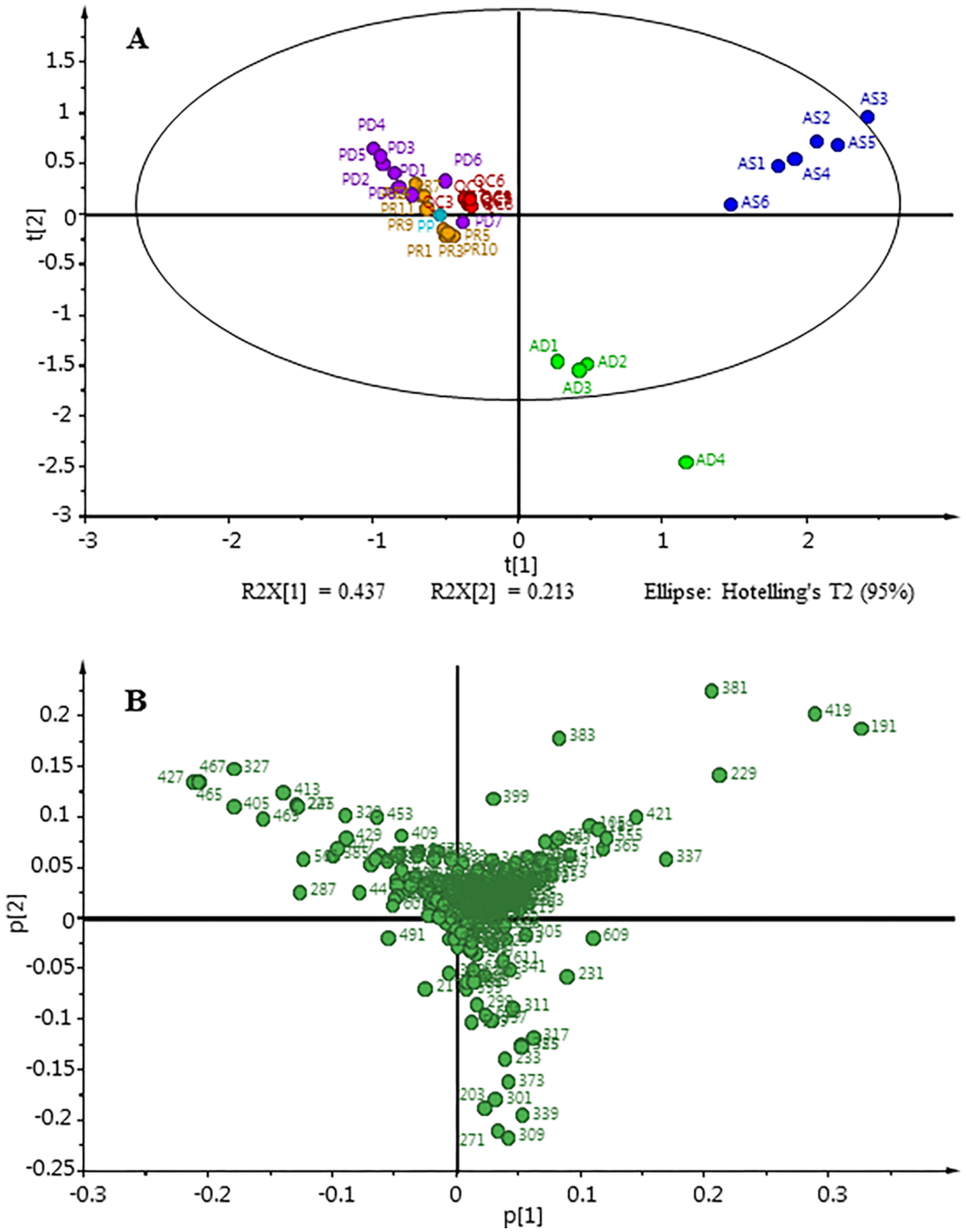

Figure 4. PCA results of DI-stepwise MIM data set for HMs-of-choice (e.g., AS1−AS6, AD1−AD4, PD1−PD8, PR1−PR11, and PP1). (A) Score scatting plot, where quality control samples tightly gather and the other samples are clustered as three classes (Class I, blue dots for AS1−AS6; Class II, purple dots for PD1−PD8, orange dots for PR1−PR11, and turquoise dot for PP1; and Class III, green dots for AD1−AD4). (B) Loading plot, and each dot is coded by Q1 ion of MIM ion transition.

flow rate would dampen the metabolite coverage, while a great flow rate would result in the saturation of the electron multiplier at the back of Q3 cell.[30] Flow rates ramped from 2 to 50 μL/min (step size as 2 μL/min) were carefully evaluated. The primary signals were involved to assay the dynamic range by constructing the intensity vs. flow rate curves. The signals including m/z 327, 337, 381, 427, 465, 467, and 469 significantly deviated from the regressive calibration curves when the flow rate was greater than 10 μL/min. In the case of flow rate as 10 μL/min, the signal coverage was comparable with that of 20 μL/min and, nonetheless, significantly greater (18.3%) than that of 6 μL/min. The flow rate as 10 μL/min was ultimately applied for the syringe pump.

Regarding the second dimension, all fragment ions produced by EPI scans are overlaid in Figure 2 and all the detailed information is illustrated in Table S2. Each fragment ion species corresponded to a dot. Signals including m/z 175, 191, 203, 227, 245, 327, 381, and 425 exhibited a great occurrence rate. As aforementioned, m/z 203, 227, 245, and 327 could be generated by a large array of angular-type pyranocoumarins. Actually, this panel of fragment ions could be also sourced from linear-type pyranocoumarins (Figure S3B) and angular-type furanocoumarins (Figure S3C). However, as the

https://dx.doi.org/10.1021/acs.analchem.0c00483
Anal. Chem. 2020, 92, 7646−7656

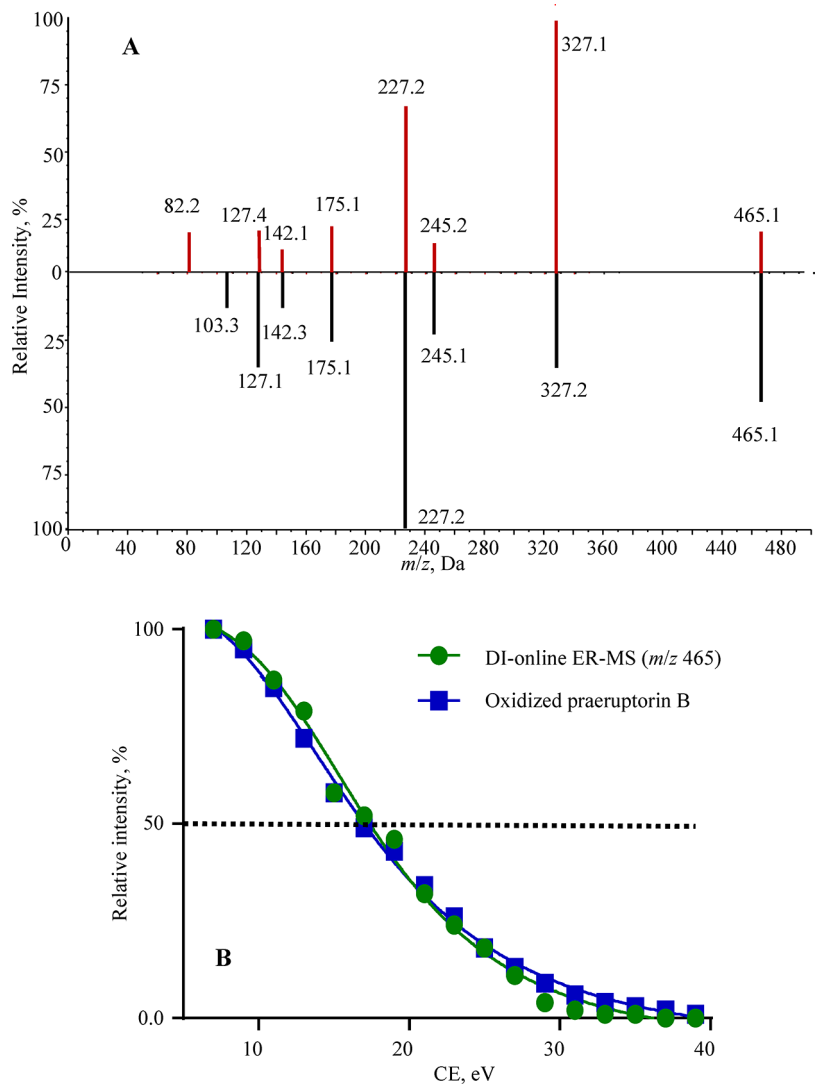

Figure 5. (A) MS^2 spectrum of m/z 465 acquired by DI-MIM-IDA-EPI (downer) as well as the reference MS^2 spectrum of oxidized praeruptorin B (m/z 465) in the in-house data library (upper), and great matching rate occurs between the two spectra. (B) Breakdown graph matching between m/z 465 = 465 acquired by online ER-MS (dot; (equation: $Y = -0.07421 + 1.11521/(1 + X^{3.687})/17.65^{3.687}$) and CE_{50}: 17.65 eV) and oxidized praeruptorin B (m/z 465 = 465) acquired by LC−Qtrap-MS (square; (equation: $Y = -0.07724 + 1.15224/(1 + X^{3.128})/17.55^{3.128}$) and CE_{50}: 17.55 eV), and the two regressive curves exhibit great similarity.

diagnostic ions of linear-type furanocoumarins, e.g., nodakenin is a feature compound of Angelicae decursiva Radix, m/z 247 and 229 signals (Figure S3D) were seldom observed, indicating a low occurrence rate of linear-type furanocoumarins in the HMs-of-choice. The significant distributions of m/z 191 and 381 could be tentatively attributed to the dissociation of ligustilide oligomers. Regarding a given ligustilide dimer, e.g., tokinolide B,[38] the observation of m/z 191 was initiated by retro-Diels−Alder fission (Figure S3E).

The breakdown graphs of all MIM ion transitions were harvested from an online ER-MS program (3rd dimension). The overlaid MIM fingerprints vs. stepped CEs are illustrated as Figure 3A, and actually, a total of 285 breakdown graphs are included in this figure. The breakdown graph could be constructed for each MIM ion transition, actually Q1 ion, by individually exacting the corresponding PIT set. Almost all ion transitions received minor responses at CE > 31 eV. For most ion transitions, their responses decreased with the increment of CE. Taking m/z 381 for instance, the greatest intensity occurred at a low CE level (5, 7, and 9 eV), and its breakdown graph (Figure 3B) could be fitted by a sigmoid curve with Graphpad Prism software. However, a couple of signals received Gaussian-type breakdown graphs, m/z 227 for instance (Figure 3C), because these signals were actually fragment ion species that originated from an array of angular-type pyranocoumarins through ion-source dissociation. Moreover, selected MIM ion transitions, such as m/z 381, 383, 385, 405, 409, 427, 445, and 465 (only show Q1 ions), were employed to evaluate the interinjection variations (RSDs %) of CE_{50}. Among six direct injections, mild variations were observed for the targeted ions, such as m/z 381 (1.8%), 383 (2.1%), 385 (1.6%), 405 (2.9%), 409 (2.5%), 427 (2.2%), 445 (2.3%), and 465 (2.5%).

Chemome Comparison Among Confusing HMs. MIM fingerprints of those homogenized samples are shown in Figure S4. Some visible differences could be found among the subfigures. MIM features, such as m/z 105, 189, 191, 219, 229, 231, 263, 267, 319, 337, 365, 381, 419, 525, 543, and 555, existed as the primary signals of Angelicae sinensis Radix (Figure S4A). The signals including m/z 189, 191, 203, 219,

https://dx.doi.org/10.1021/acs.analchem.0c00483
Anal. Chem. 2020, 92, 7646−7656

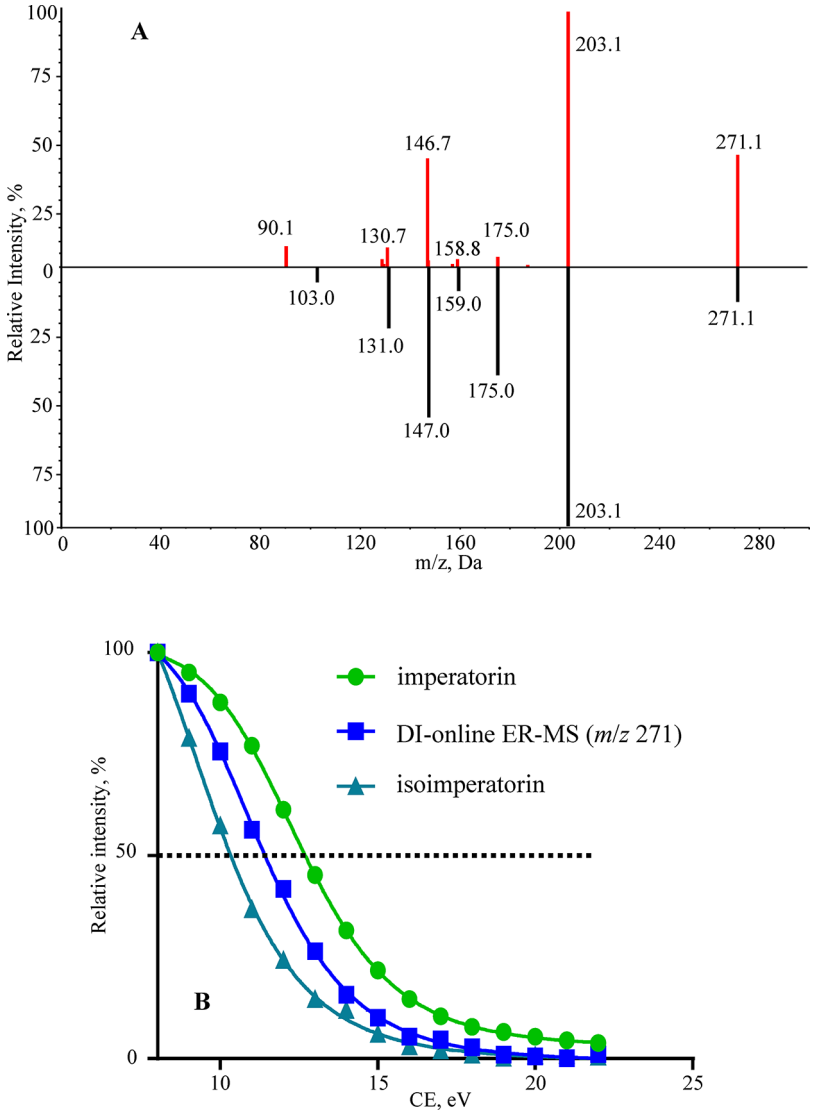

Figure 6. (A) MS^2 spectrum of m/z 271 acquired by MIM-IDA-EPI (downer) as well as the reference MS^2 spectrum of imperatorin/isoimperatorin (m/z 271) in the data library (upper), and great similarity occurs between the two spectra. (B) Breakdown graph of m/z 271 = 271 acquired by DI-online ER-MS (square; (equation: $Y = -0.00592 + 1.08092/(1 + X^{7.53})/11.22^{7.53}$) and CE_{50}: 11.22 eV) locating between the reference breakdown graphs (m/z 271 = 271) of imperatorin (dot; (equation: $Y = 0.02975 + 0.98825/(1 + X^{8.153})/12.54^{8.153}$) and CE_{50}: 12.54 eV) and isoimperatorin (triangle; (equation: $Y = -0.004892 + 1.294892/(1 + X^{6.632})/9.651^{6.632}$) and CE_{50}: 9.65 eV).

231, 233, 271, 287, 301, 309, 311, 317, 319, 325, 337, 339, 341, 343, 355, 357, 365, 373, 381, 383, and 543 dominated the Angelicae dahuricae Radix fingerprint (Figure S4B). Angelicae decursiva Radix were rich of m/z 221, 227, 245, 287, 327, 381, 383, 385, 413, 415, 405, 427, 429, 463, 465, 467, 469, 543, and 561 signals (Figure S4C). Either Peucedani Radix (Figure S4D) or Peucedani pubescens Radix (Figure S4E) assigned significant intensities to m/z 227, 245, 327, 329, 337, 381, 383, 409, 427, 465, 467, 469, 561, 601, and 603. Overall, most of the primary signals could be found as quasi-molecular ions in Table S1, whereas some signals, e.g., 227, 245, and 327, existed as fragment ion species.

Afterward, the quantitative data set of Group I samples was imported into SIMCA-P software for multivariate statistical analysis. The score scattering plot of PCA is yielded as Figure 4A. The nine-component model explained 99.8% of the variances, and the first two principal components accounted for 65.0% (43.7% for first principal component and 21.3% for second principal component). Obviously, all QC samples (red dots) tightly gathered near to the original point, as expected, indicating that DI-stepwise MIM owned great precision. Dramatic differences occurred among different species, and two samples, such as AS3 and AD4, were distributed out of Hotelling's T^2 ellipse (95%). All samples were sorted into three classes, including Class I (blue dots, AS1−AS6) in first quadrant, Class II (purple dots for PD1−PD8, orange dots for PR1−PR11, and turquoise dot for PP1) spanning both second and third quadrants, and Class III (green dots, AD1−AD4) in fourth quadrant. The first principal component was able to completely differentiate Class III from Class I, whereas the second principal component enabled discriminating Class II from Classes I and III. Regarding the loading plot (Figure 4B), some variables such as m/z 191, 419, 381, 229, 383, 337, and 421 from first quadrant, m/z 427, 465, 467, 327, 405, 413, 463, 227, 245, and 409 from second quadrant, and m/z 309, 271, 339, 301, 203, 373, 233, 355, 325, and 317 from fourth quadrant, being accumulated in Classes I, II, and III, respectively, were observed as the outliers.

https://dx.doi.org/10.1021/acs.analchem.0c00483
Anal. Chem. 2020, 92, 7646−7656

Efforts were afterward devoted onto structural annotation of those potential chemical markers. These variables were carefully characterized by retrieving the MS^2 spectra and breakdown graphs in the homemade data library (Table S1). The descriptions of those dots as well as some other key information are summarized in Table S3. Overall, pyranocoumarins (e.g., prearuptorin A, praeruptorin B, and pteryxin), linear-type furanocoumarins (e.g., imperatorin and isoimperatorin), and ligustilide derivatives (e.g., ligustilide isomers and their dimers) were regarded as the determinant roles contributing to the classification pattern. Particularly, variables including m/z 227, 245, and 327 were the primary in-source fragment ions of angular-type pyranocoumarins, linear-type pyranocoumarins, and angular-type furanocoumarins, which were claimed as the primary chemical families in Angelicae decursiva Radix, Peucedani Radix, and Peucedani pubescens Radix.[30,31]

Taking m/z 465 for instance, the MS^2 spectrum containing primary signals at m/z 327, 245, 227, 175, and 127 (Figure 5A), agreed well with the reference spectrum of oxidized praeruptorin B (m/z 465, **174**) registered in the data library (Table S1). The proposed mass fragmentation pathways are depicted in Figure S5. MIM ion transition of m/z 465 = 465 was responsible for the generation of the breakdown graph with the online ER-MS program. The normalized response data file of PIT set (m/z 465.001 = 465.001, 465.002 = 465.002, and so on) was subjected to Graphpad Prism software for the construction of relative response vs. CE plots and the sigmoid-shaped breakdown graph as well. Great consistency was observed for both the regressive sigmoid curves together with CE_{50} values between the results generated from DI-online ER-MS ((equation: $Y = -0.07421 + 1.11521/(1 + X^{3.687})/17.65^{3.687}$) and CE_{50}: 17.65 eV) and the reference information ((equation: $Y = -0.07724 + 1.15224/(1 + X^{3.128})/17.55^{3.128}$) and CE_{50}: 17.55 eV) acquired by LC−Qtrap-MS (Figure 5B). The variable coded as m/z 465 was therefore denoted as oxidized praeruptorin B. On the other side, MS^2 spectrum of m/z 271 acquired by EPI experiment showed great similarity with the reference MS^2 spectrum of imperatorin/isoimperatorin (Figure 6A), including identical fragment ion species at m/z 203, 175, 159, 147, and 131. The proposed mass fragmentation pathways as well as the assignment of primary fragment ions are depicted in Figure S6. However, the regressive breakdown graph ((equation: $Y = -0.00592 + 1.08092/(1 + X^{7.53})/11.22^{7.53}$) and CE_{50}: 11.22 eV) yielded from online ER-MS exactly located between the reference ones of imperatorin ((equation: $Y = 0.02975 + 0.98825/(1 + X^{8.153})/12.54^{8.153}$) and CE_{50}: 12.54 eV) and isoimperatorin ((equation: $Y = -0.004892 + 1.294892/(1 + X^{6.632})/9.651^{6.632}$) and CE_{50}: 9.65 eV, Figure 6B). Hence, the classification ability of m/z 271 should be attributed to the combined contribution of both imperatorin and isoimperatorin.

Owing to the diagnostic fragment ions at m/z 245 and 227, m/z 405, an important outlier, was tentatively described as the isotopic ion of quasi-molecular ion (m/z 404 $[M + NH_4]^+$) of both praeruptorin A and pteryxin because they frequently served as the most abundant components in Peucedani Radix.[34] To consolidate the speculation, an additional MIM ion transition as m/z 404 = 404 was fortified into the current list and Angelicae decursiva Radix, Peucedani Radix and Peucedani pubescens Radix samples were assayed one more time. As a result, the ion transition m/z 404 = 404 generated the greatest response (Figure S7). A previous article also declaimed that adducted molecular ions could widely occur in the DI-MS fingerprint in comparison to LC−MS.[39]

Pros and Cons. High-throughput is the most popular property of DI-MS, because time-intensive LC separation is totally omitted. In the current study, a single DI-stepwise MIM measurement was merely accomplished within 4 min. Actually, there were two other merits accompanying the high-throughput advantage. Only a bit of solvent was consumed by DI-stepwise MIM via infusing a tens of microliters sample solution. The labile compounds could keep intact prior to arriving at the ion source because the long-term exposures of these components to the mobile phase (e.g., warm organic solvents) and stationary phase (e.g., hydroxyl-bearing bonded silica particles) were completely avoided.

Signal alignment is usually an annoying task before importing a data set into multivariated statistical analysis software.[5] In particular, the sizes of the compound pools and the chemical types existing in different HMs are intrinsically incomparable and the signal alignment challenge is therefore advanced. In comparison of conventional DI-MS, the data processing workload could be dramatically alleviated by DI-3D-MS, because each DI-stepwise MIM measurement always gave out a total of 285 features. Actually, this forced signal alignment strategy is theoretically similar to the binning program for ^1H NMR-based metabolomics.[40]

MIM-IDA-EPI and online ER-MS were programmed to gain the MS^2 spectra and breakdown graphs, respectively, and structural annotation for those potential chemical markers could be significantly promoted. The smart MIM-IDA-EPI program was able to record MS^2 spectrum for each Q1 ion with the DDA manner, and it was convenient to affiliate any fragment ion to its precursor ion, indicating great contributions for structural characterization. However, all HMs-of-choice were derived from *Umbelliferae* plants, resulting in the wide occurrences of isomers. Structural identification of the outliers is risked by isomers, because of their almost identical MS^2 spectra. As aforementioned, fragment ion species at m/z 203, 175, 159, 147, and 131 could not unambiguously configure the chemical structure for m/z 271. Owing to the benefits of breakdown graph matching, the contribution of this variable toward the classification pattern was assigned to both imperatorin and isoimperatorin. Similarly, because of the fragment ions (m/z 327, 245, 227, 175, and 127) and CE_{50} evidence, the primary outlier of m/z 465 was confirmatively identified as oxidized praeruptorin B. Moreover, some other potential chemical markers, for instance m/z 191, 381, and 427 signals, should be sourced from ligustilide and isomers, dimeric ligustilide and isomers, and praeruptorin B and isomers, respectively, by integrating the clues from MS^2 spectra and breakdown graphs. Therefore, the combination of MIM-IDA-EPI and online ER-MS is meaningful to strengthen the ability of DI-MS through providing orthogonal structural evidence to MS^2 spectra, notably when the advanced database containing MS^2 spectral and CE_{50} information is available in the near future.

Owing to the increasing demands of high-throughput assaying, rapid development has occurred for LC instrumentation to finish a single measurement within a couple of minutes, resulting in that the peak yielded from LC−MS being quite narrow, usually with a width of several seconds. Co-elution frequently occurs, moreover, when measuring complicated matrices, e.g., HMs and biological samples. It is subsequently a

https://dx.doi.org/10.1021/acs.analchem.0c00483
Anal. Chem. 2020, 92, 7646−7656

challenging workload to simultaneously record qualitative and quantitative information for all compounds. The chromatographic peaks usually suffer from insufficient data points even though the employment of a so-called scheduled SRM algorithm[30] and significant instrumental noise are also resulted from the limited dwell time.[41] MS^2 spectra acquired by LC−MS usually come out with low quality due to the time limitation, and even worse, MS^2 spectra of those less abundant ions may be absent in the data file. In contrary, the width of each signal generated from DI-3D-MS was theoretically equal to the whole infusion time, because each compound continuously entered the ion source. The desired dwell time, as great as 100 ms, was available for each MIM ion transition, and enough acquisition time could be also assigned to all defined EPI experiments as well. The instrumental noise was thereby dramatically suppressed due to receiving enough dwell time. Therefore, the quality of quantitative information and MS^2 spectra could be significantly improved by DI-3D-MS.

In comparison to LC−MS, there are two drawbacks for DI-3D-MS. First, the significant matrix effect is an intrinsic disadvantage owing to the ionization competition among a large panel of molecules synchronously arriving at the ion source. To evaluate the relative matrix effect, a stepwise MIM program was applied for LC−MS to measure the QC sample. The summed MIM spectrum over a measured time (0−25 min) from LC−MS was compared with DI-stepwise MIM fingerprint (Figure S8). Overall, the two fingerprints shared a set of primary signals, such as m/z 203, 227, 245, 287, 327, 329, 405, 427, 447, 449, and 451. However, significant responses occurred for m/z 149 and 271 generated from LC−MS, while signals at m/z 337, 381, 383, 385, and 561 received greater intensities from DI-stepwise MIM. Second, due to the absence of LC separation, a single MIM ion transition might correspond to several isomers. In the current study, signals such as m/z 191, 271, 405, 381, and 427, should be initiated by two or more compounds. It is impossible to definitely point out which compound should be the real contributor toward HMs discrimination, although breakdown graph matching is able to plausibly link signals with compounds. In our opinion, the two disadvantages can be addressed, to some extents, according to efficient chromatographic fractionation. The simplified samples will afterward show inferior matrix effects, and the isomer-blind defect of DI-MS will also be partially addressed.

CONCLUSION

To achieve high-throughput metabolomics, a novel strategy termed as DI-3D-MS was proposed. Stepwise MIM was programmed as the first dimension to universally acquire the quantitative information and to generate data files with a constant length (285 variables); MIM-IDA-EPI served as second dimension to record MS^2 spectra for all Q1 ions; and online ER-MS was scheduled as third dimension to yield breakdown graphs for each MIM item. The applicability was validated through chemome comparison among several confusing HMs, e.g., Angelicae sinensis Radix, Angelicae dahuricae Radix, Angelicae decursiva Radix, Peucedani Radix, and Peucedani pubescens Radix. To assist structural annotation, an in-house data library was built by involving MS^2 spectra and breakdown graphs acquired by LC−MS. The qualitative and quantitative potentials of DI-3D-MS were validated toward metabolomics study, and particularly, a single quantitative measurement merely took 4 min. Significant species differences were observed within HMs-of-choice, and the variables in response to the classification style were structurally described as angular-type pyranocoumarins, linear-type pyranocoumarins, angular-type furanocoumarins, and ligustilide derivatives by inquiring the MS^2 spectra and breakdown graphs to the in-house data library. Because of integrating stepwise MIM, MIM-IDA-EPI, and online ER-MS, 3D MS program, theoretically a new time-dependent MS/MS concept, is able to simultaneously acquire qualitative and quantitative information on a DI sample, and DI-3D-MS could serve as an auxiliary tool for conventional LC−Qtof-MS, particularly toward rapid metabolomics.

ASSOCIATED CONTENT

Supporting Information

The Supporting Information is available free of charge at https://pubs.acs.org/doi/10.1021/acs.analchem.0c00483.

Tables of in-house data library, MS^2 spectral information, and information for potential chemical markers and figures of overlaid TIC chromatograms, LC−IT-TOF-MS chromatograms, proposed mass fragmentation pathways, and mass spectra fingerprints (PDF)

AUTHOR INFORMATION

Corresponding Authors

Yuelin Song − *Modern Research Center for Traditional Chinese Medicine, School of Chinese Materia Medica, Beijing University of Chinese Medicine, Beijing 100029, China;* orcid.org/0000-0001-9431-6257; Email: syltwc2005@163.com

Jun Li − *Modern Research Center for Traditional Chinese Medicine, School of Chinese Materia Medica, Beijing University of Chinese Medicine, Beijing 100029, China;* orcid.org/0000-0001-8243-5267; Email: drlj666@163.com

Authors

Xia Xu − *Modern Research Center for Traditional Chinese Medicine, School of Chinese Materia Medica, Beijing University of Chinese Medicine, Beijing 100029, China*

Wei Li − *Modern Research Center for Traditional Chinese Medicine, School of Chinese Materia Medica, Beijing University of Chinese Medicine, Beijing 100029, China*

Ting Li − *Modern Research Center for Traditional Chinese Medicine, School of Chinese Materia Medica, Beijing University of Chinese Medicine, Beijing 100029, China*

Ke Zhang − *Modern Research Center for Traditional Chinese Medicine, School of Chinese Materia Medica, Beijing University of Chinese Medicine, Beijing 100029, China*

Qingqing Song − *Modern Research Center for Traditional Chinese Medicine, School of Chinese Materia Medica, Beijing University of Chinese Medicine, Beijing 100029, China*

Li Liu − *Guizhou Hanfang Pharmaceutical Co. Ltd., Guiyang 550014, China*

Pengfei Tu − *Modern Research Center for Traditional Chinese Medicine, School of Chinese Materia Medica, Beijing University of Chinese Medicine, Beijing 100029, China;* orcid.org/0000-0003-3553-1840

Yitao Wang − *State Key Laboratory of Quality Research in Chinese Medicine, Institute of Chinese Medical Sciences, University of Macau, Taipa 999078, Macao*

Complete contact information is available at: https://pubs.acs.org/10.1021/acs.analchem.0c00483

https://dx.doi.org/10.1021/acs.analchem.0c00483
Anal. Chem. 2020, 92, 7646−7656

Notes

The authors declare no competing financial interest.

■ ACKNOWLEDGMENTS

This work was financially supported by the National Natural Science Foundation of China (Nos. 81773875 and 81530097), Young Elite Scientists Sponsorship Program by China Association for Science and Technology (No. 2017QNRC001), Young Scientist Program by Beijing University of Chinese Medicine (No. BUCM-2019-QNKXJB006), the Macao Science and Technology Development Fund (No. 071/2017/A2), and Guizhou Hanfang Pharmaceutical Co. Ltd.

■ REFERENCES

(1) Liu, X. Y.; Zhou, L. N.; Shi, X. Z.; Xu, G. W. *TrAC, Trends Anal. Chem.* **2019**, *121*, 115665.
(2) Dettmer, K.; Aronov, P. A.; Hammock, B. D. *Mass Spectrom. Rev.* **2007**, *26*, 51−78.
(3) Villas-Boas, S. G.; Mas, S.; Akesson, M.; Smedsgaard, J.; Nielsen, J. *Mass Spectrom. Rev.* **2005**, *24*, 613−646.
(4) Khamis, M. M.; Adamko, D. J.; El-Aneed, A. *Mass Spectrom. Rev.* **2017**, *36*, 115−134.
(5) Wang, Y.; Ma, L.; Zhang, M.; Chen, M.; Li, P.; He, C.; Yan, C.; Wan, J. B. *J. Chromatogr. Sci.* **2019**, *57*, 9−16.
(6) Johnson, K. J.; Wright, B. W.; Jarman, K. H.; Synovec, R. E. *J. Chromatogr. A* **2003**, *996*, 141−155.
(7) Kind, T.; Wohlgemuth, G.; Lee, D. Y.; Lu, Y.; Palazoglu, M.; Shahbaz, S.; Fiehn, O. *Anal. Chem.* **2009**, *81*, 10038−10048.
(8) Zhang, Z. *J. Am. Soc. Mass Spectrom.* **2012**, *23*, 764−72.
(9) Wu, J.; McAllister, H. *J. Mass Spectrom.* **2003**, *38*, 1043−1053.
(10) Olsen, J. V.; de Godoy, L. M.; Li, G.; Macek, B.; Mortensen, P.; Pesch, R.; Makarov, A.; Lange, O.; Horning, S.; Mann, M. *Mol. Cell. Proteomics* **2005**, *4*, 2010−2021.
(11) Wang, L.; Su, B.; Zeng, Z.; Li, C.; Zhao, X.; Lv, W.; Xuan, Q.; Ouyang, Y.; Zhou, L.; Yin, P.; Peng, X.; Lu, X.; Lin, X.; Xu, G. *Anal. Chem.* **2018**, *90*, 11401−11408.
(12) Luo, P.; Yin, P.; Zhang, W.; Zhou, L.; Lu, X.; Lin, X.; Xu, G. *J. Chromatogr. A* **2016**, *1437*, 127−136.
(13) Luo, P.; Dai, W.; Yin, P.; Zeng, Z.; Kong, H.; Zhou, L.; Wang, X.; Chen, S.; Lu, X.; Xu, G. *Anal. Chem.* **2015**, *87*, 5050−5055.
(14) Chen, S.; Kong, H.; Lu, X.; Li, Y.; Yin, P.; Zeng, Z.; Xu, G. *Anal. Chem.* **2013**, *85*, 8326−8333.
(15) Xia, Y. Q.; Ciccimaro, E.; Zheng, N.; Zhu, M. *Bioanalysis* **2017**, *9*, 183−192.
(16) Yao, M.; Ma, L.; Duchoslav, E.; Zhu, M. *Rapid Commun. Mass Spectrom.* **2009**, *23*, 1683−1693.
(17) Yao, M.; Ma, L.; Humphreys, W. G.; Zhu, M. *J. Mass Spectrom.* **2008**, *43*, 1364−1375.
(18) Chen, W.; Gong, L.; Guo, Z.; Wang, W.; Zhang, H.; Liu, X.; Yu, S.; Xiong, L.; Luo, J. *Mol. Plant* **2013**, *6*, 1769−1780.
(19) Huan, T.; Tang, C.; Li, R.; Shi, Y.; Lin, G.; Li, L. *Anal. Chem.* **2015**, *87*, 10619−10626.
(20) Li, L.; Li, R.; Zhou, J.; Zuniga, A.; Stanislaus, A. E.; Wu, Y.; Huan, T.; Zheng, J.; Shi, Y.; Wishart, D. S.; Lin, G. *Anal. Chem.* **2013**, *85*, 3401−3408.
(21) Wishart, D. S.; Feunang, Y. D.; Marcu, A.; Guo, A. C.; Liang, K.; Vazquez-Fresno, R.; Sajed, T.; Johnson, D.; Li, C.; Karu, N.; Sayeeda, Z.; Lo, E.; Assempour, N.; Berjanskii, M.; Singhal, S.; Arndt, D.; Liang, Y.; Badran, H.; Grant, J.; Serra-Cayuela, A.; Liu, Y.; Mandal, R.; Neveu, V.; Pon, A.; Knox, C.; Wilson, M.; Manach, C.; Scalbert, A. *Nucleic Acids Res.* **2018**, *46*, D608−D617.
(22) Horai, H.; Arita, M.; Kanaya, S.; Nihei, Y.; Ikeda, T.; Suwa, K.; Ojima, Y.; Tanaka, K.; Tanaka, S.; Aoshima, K.; Oda, Y.; Kakazu, Y.; Kusano, M.; Tohge, T.; Matsuda, F.; Sawada, Y.; Hirai, M. Y.; Nakanishi, H.; Ikeda, K.; Akimoto, N.; Maoka, T.; Takahashi, H.; Ara, T.; Sakurai, N.; Suzuki, H.; Shibata, D.; Neumann, S.; Iida, T.; Tanaka, K.; Funatsu, K.; Matsuura, F.; Soga, T.; Taguchi, R.; Saito, K.; Nishioka, T. *J. Mass Spectrom.* **2010**, *45*, 703−714.
(23) Sun, Z.; Song, J.; Zhang, X.; Wang, A.; Guo, Y.; Yang, Y.; Wang, X.; Xu, K.; Deng, J. *BioMed Res. Int.* **2018**, *2018*, 1.
(24) Dubbelman, A. C.; Cuyckens, F.; Dillen, L.; Gross, G.; Vreeken, R. J.; Hankemeier, T. *Anal. Chim. Acta* **2018**, *1020*, 62−75.
(25) Wang, Y.; Feng, R.; Wang, R.; Yang, F.; Li, P.; Wan, J. B. *Anal. Chim. Acta* **2017**, *992*, 67−75.
(26) Yan, Z.; Yan, R. *Anal. Chem.* **2015**, *87*, 2861−2868.
(27) Song, Q. Q.; Li, J.; Huo, H.; Cao, Y.; Wang, Y.; Song, Y.; Tu, P. *Anal. Chem.* **2019**, *91*, 15040−15048.
(28) Cao, Y.; Chai, C.; Chang, A.; Xu, X.; Song, Q.; Liu, W.; Li, J.; Song, Y.; Tu, P. *J. Chromatogr. A* **2020**, *1609*, 460515.
(29) Liu, W.; Cao, Y.; Ren, Y.; Xu, X.; He, L.; Xia, R.; Tu, P.; Wang, Y.; Song, Y.; Li, J. *J. Chromatogr. A* **2020**, *1617*, 460827.
(30) Song, Y. L.; Song, Q. Q.; Liu, Y.; Li, J.; Wan, J. B.; Wang, Y. T.; Jiang, Y.; Tu, P. F. *Anal. Chim. Acta* **2017**, *953*, 40−47.
(31) Tao, Y.; Luo, J.; Lu, Y.; Xu, D.; Hou, Z.; Kong, L. *Nat. Prod. Commun.* **2009**, *4*, 1079−1084.
(32) Li, B.; Zhang, X.; Wang, J.; Zhang, L.; Gao, B.; Shi, S.; Wang, X.; Li, J.; Tu, P. *Phytochem. Anal.* **2014**, *25*, 229−240.
(33) Chinese Pharmacopoeia Committee. *The Pharmacopoeia of the People's Republic of China*; Chinese Medical Science and Technology Press: Beijing, China, 2015; Vol. *I*, pp 105−338.
(34) Song, Y. L.; Jing, W. H.; Du, G.; Yang, F. Q.; Yan, R.; Wang, Y. T. *J. Chromatogr. A* **2014**, *1338*, 24−37.
(35) Zhao, Y.; Sun, J.; Yu, L. L.; Chen, P. *Anal. Bioanal. Chem.* **2013**, *405*, 4477−4485.
(36) Song, Y. L.; Zhang, N.; Shi, S. P.; Li, J.; Zhao, Y. F.; Zhang, Q.; Jiang, Y.; Tu, P. F. *J. Chromatogr. A* **2015**, *1406*, 136−144.
(37) Song, Y.; Yan, H.; Chen, J.; Wang, Y.; Jiang, Y.; Tu, P. *J. Pharm. Biomed. Anal.* **2014**, *89*, 183−196.
(38) Zhang, Q.; Huo, M.; Zhang, Y.; Qiao, Y.; Gao, X. *J. Chromatogr. A* **2018**, *1552*, 17−28.
(39) Lin, L.; Yu, Q.; Yan, X.; Hang, W.; Zheng, J.; Xing, J.; Huang, B. *Analyst* **2010**, *135*, 2970−2978.
(40) Anderson, P. E.; Reo, N. V.; DelRaso, N. J.; Doom, T. E.; Raymer, M. L. *Metabolomics* **2008**, *4*, 261−272.
(41) Song, Q. Q.; Song, Y. L.; Zhang, N.; Li, J.; Jiang, Y.; Zhang, K. R.; Zhang, Q.; Tu, P. F. *RSC Adv.* **2015**, *5*, 57372−57382.

https://dx.doi.org/10.1021/acs.analchem.0c00483
Anal. Chem. 2020, 92, 7646−7656